JOURNAL OF APPLIED ELECTROCHEMISTRY 21 (1991) 395–401

Characterization of gas flow configurations for phosphoric acid fuel cells

K. MITSUDA, T. MURAHASHI

Central Research Laboratory, Mitsubishi Electric Corporation, Tsukaguchi-honmachi 8-1-1, Amagasaki-shi, Hyogo 661, Japan

Received 15 February 1990; revised 27 September 1990

The cell performance and polarization distribution in the horizontal plane of a phosphoric acid fuel cell (PAFC) were studied for thirteen different types of gas flow. In all cases, the potentials of the anode and cathode in the fuel outlet area shifted to positive directions. At 90% utilization of fuel, the potential shift and the cell voltage changed significantly from one type to another. Experimental results show that the cell voltage increased, and the potential shift decreased in the following order; CROSS-FLOW < RETURN-FLOW = CO-FLOW < COUNTER-FLOW < type E2. The extent of the change between various types depended on the following three conditions. (1) The fuel gas has an opportunity to be used twice in the horizontal plane of a cell. (2) The fuel gas flow is in parallel with the air flow. (3) The fuel gas flow is opposite to the air flow. These are requirements for obtaining good and stable performance of a fuel cell. The CROSS-FLOW case has none of these three conditions, the RETURN-FLOW case has the first condition, the CO-FLOW case has the second, the COUNTER-FLOW case has the second and the third conditions, and the best gas flow type (type E2) has all.

1. Introduction

Several types of gas flows have been proposed for the supply of reactant gases to phosphoric acid fuel cells. CROSS-FLOW [1, 2] is the simplest and the most general type, where the fuel and air flows are at right angles. RETURN-FLOW [3, 4] is also a popular type of gas flow, in which the direction of fuel is reversed in a cell plane using a gas manifold [5]. CO-FLOW [6, 7] and COUNTER-FLOW [8] types in which the fuel and air flows are parallel, are somewhat hard to construct, requiring an internal gas manifold.

There are several modeling studies in the literature [8–10], but very few experimental ones, and none that can be used for direct comparison of these flow types. This paper reports a systematic experimental study of configuration effects in fuel cells.

The homogeneous distribution of current in the plane parallel to the matrix layer of a cell has been the ultimate goal for the best cell performance. In practical fuel stacks, because of the large scale, the current distribution is considered to be affected by both the reactant gas composition (mainly cathode side) and temperature distributions [8]. However, the results of recent work [12, 13] indicates that the current distribution can also be affected by the local acidity (pH) change of electrolyte due to increase of fuel utilization.

Recent work reported the inhomogeneous distribution of polarization in the horizontal plane of a PAFC using a single cell equipped with four reversible hydrogen electrodes for reference (RHEs) [12, 13]. Shifts of the cathode and anode potentials in the positive direction were observed in the fuel outlet area. These shifts were increased by increase in hydrogen utilization. The RHE potential in the fuel outlet area shifted in the negative directions versus the potential of RHE in the fuel inlet area, and the changes corresponded to the shifts of the cathode and anode potentials in the fuel outlet area. These results indicate that the acidity of electrolyte of a PAFC can change locally due to increased fuel utilization. When fuel utilization increases, the cathode potential in the fuel outlet area becomes the most positive potential and cathode carbon corrosion can occur locally in the fuel outlet area [14, 15]. In fact, carbon corrosion of PAFC was more often observed at the cathode side components (carbon catalyst support, its substrate and the carbon bipolar plate), and especially at places opposite the fuel outlet area [16].

In order to increase the efficiency of PAFC electric power, the fuel utilization should be increased as much as possible (more than 85% is desirable). However, the increase of fuel utilization invites a risk of carbon corrosion. Accordingly, optimization of gas flow configuration is necessary to achieve the operation of PAFC at high fuel utilization. This will be suggested in this paper.

In this work, the characterization of thirteen types of gas flow in the horizontal plane of a cell is conducted using single cells furnished with twelve reference electrodes. The CROSS-FLOW, RETURN-FLOW, CO-FLOW and COUNTER-FLOW, which are well known types, are included in the thirteen types. In all cases, potential shifts were always observed in the fuel

0021-891X/91 $03.00 + .12 © 1991 Chapman and Hall Ltd.

outlet area. The height of the potential shift is a barometer of carbon corrosion. From the point of view of cell performance and corrosion resistance, RETURN-FLOW was superior to CROSS-FLOW, CO-FLOW was nearly equally good to RETURN-FLOW, and COUNTER-FLOW was superior to CO-FLOW. However, better types of gas flow in the horizontal plane of a cell (E1, E2, F1 and F2 types) were found in this work.

The relation between potential shift and cell voltage and the characterization of the thirteen types of gas flow are discussed.

2. Experimental details

Figure 1 shows the horizontal view of the anode carbon plate and the directions of fuel gas flow. The gas manifold and channels of the anode carbon plate are separated into two partitioned spaces by filling the channel in the middle with matrix sheet materials. Two sets of fuel inlets and outlets are attached on the anode carbon plate, while the cathode carbon plate has only one space and one inlet and outlet. The operation temperature was kept at 190° C by on-off control of four heaters which were set behind the carbon plates. Accordingly, the effect of temperature distributions in the plane of a cell is not considered in this work. The fabrication of the electrodes and the configuration of a single cell were the same as in a previous publication [13, 14].

Figure 2 shows the location of the reference electrodes. The dimensions of the cathode, the anode and the matrix were 100 cm^2, 144 cm^2 and 225 cm^2, respectively. The diameter of the reference electrode was 0.6 cm (0.3 cm^2). Twelve reference electrodes were embedded in the cathode carbon plate. Reversible hydrogen electrodes (RHE) were used as the reference electrode, numbered R1, R2, R3 . . . , R12. The air flow direction relative to the reference electrodes was fixed as shown in Fig. 2 in all cases, while the directions of fuel gas flow for Fuel 1 and Fuel 2 were changed. Figure 2 shows the case of the 'A1' type. The fuel exhaust gas was passed through a gas wash bottle to prevent contamination by air from the fuel outlet.

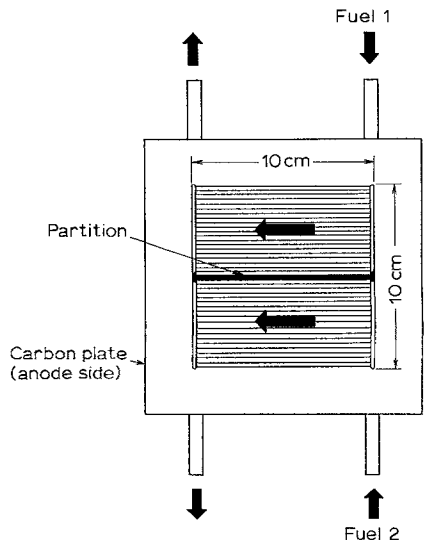

Fig. 1. Schematic illustration of the anode carbon plate and the directions of fuel gas flow.

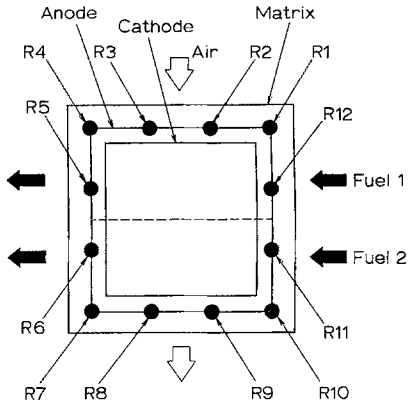

Fig. 2. The arrangement of twelve reference electrodes and the directions of gas flows.

Figure 3 shows a cross-sectional view of the cell near a reference electrode. Gold wire of 0.3 mm in diameter embedded in a Teflon™ tube was used as the lead wire. The head of this wire was flattened so as to make contact with the reference electrode. Hydrogen was supplied to the reference electrode using a Teflon™ tube embedded in the cathode carbon plate. The cathode and anode were sealed with Teflon™ gaskets. The matrix sheet was made of SiC and PTFE particles, and was fabricated by a roller press method. The average thickness was 200 μm, and two matrix sheets were used as the matrix layer in this experiment.

The single cell in which the fuel gas flow and air flow were at right angles was named the "AF cross cell", and that in which both fuel and air flow were parallel was named the "AF parallel cell". These cells were operated at atmospheric pressure.

Air or oxygen was used as the oxidant, and SRG (H_2 80% + CO_2 20%) or pure hydrogen was used as the fuel. The flow rate of the fuel was kept so as to give a fixed hydrogen utilization of SRG (mainly 90%), and the flow rate of the oxidant was set to give a fixed oxygen utilization of air of 60%, both at 200 mA cm^{-2}.

The voltage terminals of the anode and cathode plates were named A and C, respectively. Voltages between A and C, A and Rx and Rx and C (x = 1, 2, . . . , 12), were measured with a recorder (TR2731, 2741; Takeda Riken Industry Co. Ltd.).

Ohmic loss was measured using a current interruption method on a Miliohmmeter (VP-2811A, Matsushita Communication Industrial Co. Ltd.) at 200 mA cm^{-2} and the voltages were corrected to yield iR-free values. For measurement of the ohmic loss, a current of 100 mA cm^{-2} passed through the current collectors behind the carbon plates was interrupted and the rapid change of voltage (within 1 ms) was recorded. For the measurements using the Miliohmmeter (alternating current four-terminal method), the current probes were set at the current collectors, and the voltage probes were set at each voltage terminal, and the electric resistance at 200 mA cm^{-2}

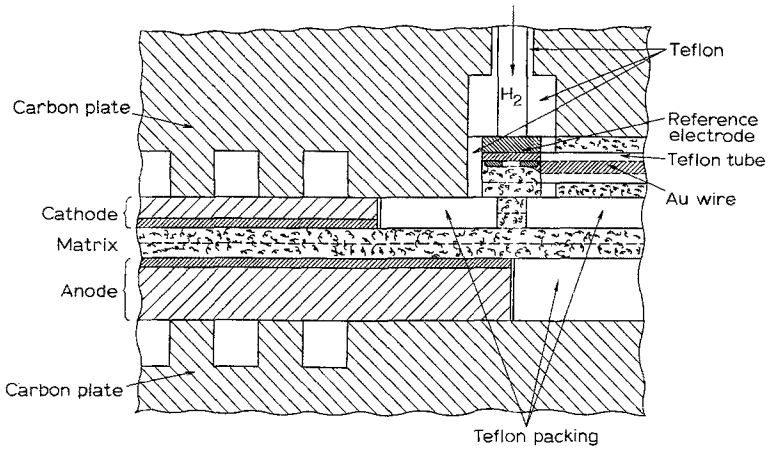

Fig. 3. Cross-sectional view showing the position of cathode, anode and reference electrode near a reference electrode.

was measured. The ohmic loss of A–Rx or Rx–Ry was always very small (within 1 mV at 100 mA cm^{-2}) and that of C–A or C–Rx was about 70 mV at 200 mA cm^{-2}. There was little difference in the plane of a cell. The cell voltages (C–A) were corrected into iR-free values, but the cathode and anode potentials were not corrected.

Details of the flow types studied are described in section 3.2.

3. Results

3.1. *The potential changes in CROSS-FLOW (A1 Type)*

Since CROSS-FLOW (Fig. 2) is the simplest and most conventional flow type, the potential behaviour of this type was investigated in detail first.

Figure 4 shows the potentials of the anode and cathode against RHE at various positions marked in the x-axis under the open circuit condition. Here, R4 is located in the fuel outlet and air inlet corner and designated as O/I. In a similar way, R1, R7 and R10 are indicated as I/I, O/O and I/O, respectively. H_2/O_2 or SRG/Air were used as reactant gases. As shown in Fig. 4, the cathode and anode potentials stay constant in the horizontal plane of a cell.

Figure 5 shows the potentials at 200 mA cm^{-2}. When H_2/O_2 were used as reactant gases, the cathode and anode potentials were constant in the horizontal plane. However, when SRG/Air were used as reactant gases, the cathode and anode potentials from R3 to R8 shifted significantly in the positive direction. The reference electrodes from R3 to R8 were located in the fuel outlet area as shown in Fig. 2, and the potential shift in the fuel outlet area increased with increase in hydrogen utilization. This behaviour was consistent with previous results for single cells each with four reference electrodes [12, 13]. Especially when the hydrogen utilization of SRG was raised to 90%, the cathode potential at R5 became higher than that of H_2/O_2.

The relations between the potential shift and the cell voltage were also investigated by changing the flow rate of fuel. The utilization of air was constant at 60%, and the utilization of fuel was set between 20%

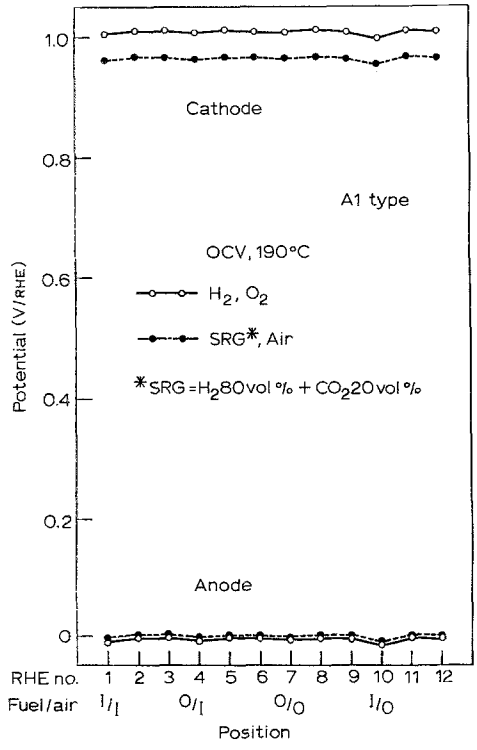

Fig. 4. Potential against RHE of cathode and anode at OCV.

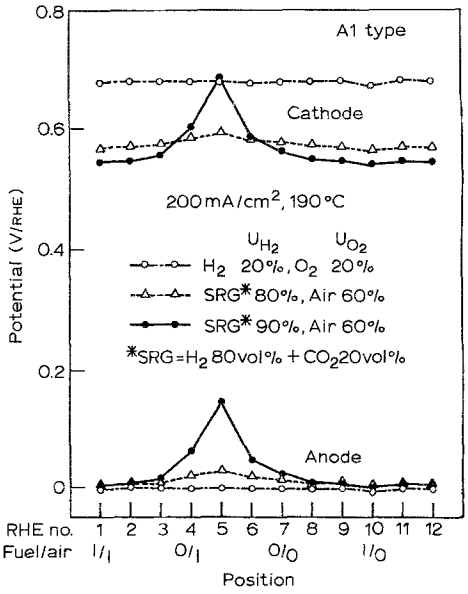

Fig. 5. Potential against RHE of cathode and anode at 200 mA cm^2.

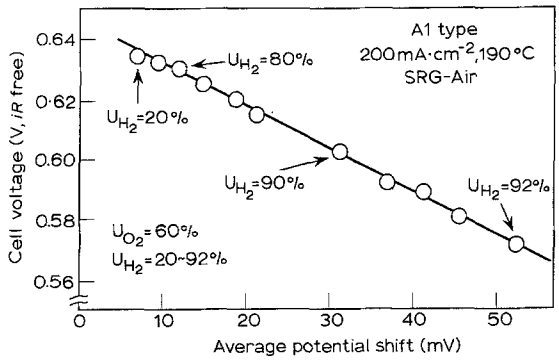

Fig. 6. The relation between average potential shift and cell voltage in the case of A1 type.

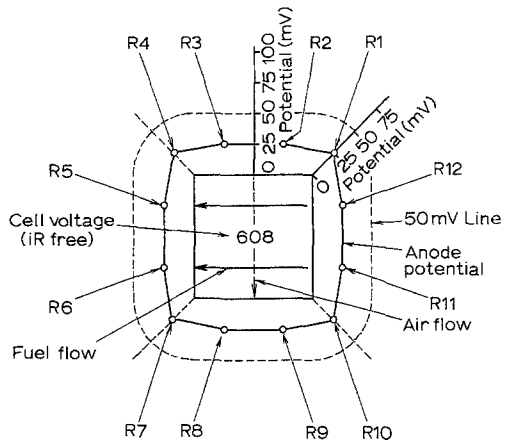

Fig. 7. Typical schematic diagram showing anode potential distribution in a plane.

and 92%. Figure 6 shows the relationship between the average potential shift with respect to the minimum anode potential and the cell voltage. The x-axis shows the average value of the potential shift at the twelve positions. The linear relation indicates that the current distributions in the plane of a cell is affected by increase of the potential shift in the fuel outlet area.

3.2. *Comparison of the thirteen gas flow types*

The characterization of the results of the thirteen different flow types are described by use of diagrams typically depicted in Fig. 7. Here, the square in the centre of the diagram shows the electrode. The cell voltage (iR-free; mV) is given in the centre of the square. The direction of airflow is shown by a broken arrow, and the directions of fuel flow in the separated portions are given by solid arrows. Each of the dots surrounding the square indicates the anode potential against an RHE at each position by the distance from the square of the cell. Namely, the four sides of the square gives 0 mV against RHE, and the outer broken line encircling the square gives the position of 50 mV against RHE. For the case of Fig. 7, as an example, twelve small circlets around the square indicate the anode potential values of 25 mV against RHE.

Figure 8 shows the results for the cases of 90% hydrogen utilization for the six types of gas flow where fuel and air are crossed at right angles (AF cross cell), and Fig. 9 shows those for the seven types of gas flow where fuel and air are parallel (AF parallel cell). The broken line which links the solid arrows schematically shows the pipe connecting the flows, for which Teflon™ tube and silicon rubber tube were used. The C1 type flow and the C2 type flow are called "RETURN-FLOW". The D1 type flow and C2 type flow are called "RETURN-FLOW". The D1 type is called "CO-FLOW" and D2 type is called "COUNTER-FLOW". In all cases, potential shifts were always observed in the fuel outlet area.

The results of Fig. 8 and Fig. 9 are summarized in Table 1. The fourth column of Table 1 shows the cell voltage (iR-free; mV). The fifth and sixth column show the maximum value of the cathode and anode potentials in each case, respectively. The cell voltage including ohmic loss (C–A) can be calculated to subtract the sixth column (A–Rx) from the fifth column (C–Rx). The seventh column shows the average potential shift, and the last column (CONDITION) is explained in section 4.2.

Figure 10 shows the relation between average

Table 1. Summary of the results of comparative experiments

	Flow type	*Name*	*Cell voltage iR free*	*Cathode potential max (mV)*	*Anode potential max (mV)*	*Average potential shift (mV)*	*Condition*		
							1	*2*	*3*
Air ⊥ Fuel	A1	CROSS	608	687	146	28	x	x	x
	A2		607	604	58	21	x	x	x
	B1		625	604	44	15	o	x	x
	B2		625	606	48	14	o	x	x
	C1	RETURN 1	620	605	52	14	o	x	x
	C2	RETURN 2	625	601	42	15	o	x	x
Air ∥ Fuel	D1	CO-FLOW	625	626	70	19	x	o	x
	D2	COUNTER	628	611	50	16	x	o	o
	D3		627	597	38	15	x	o	△
	E1		628	602	41	13	o	o	x
	E2		629	600	38	12	o	o	o
	F1		627	598	38	13	o	o	△
	F2		628	599	38	12	o	o	△

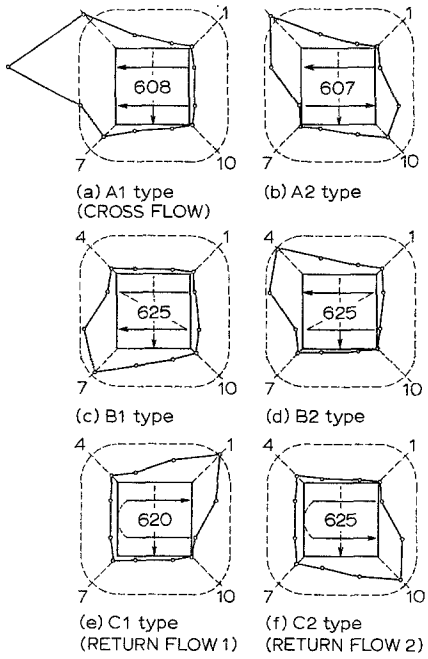

Fig. 8. Schematic diagrams showing anode potential distribution in a plane for the case of AIR ⊥ FUEL.

potential shifts and cell voltages of the thirteen gas flow types. Black and white circles represent the case of "AF cross cell" at 80% and 90% hydrogen utilization, respectively. Black and white triangles represent the cases of "AF parallel cell" at 80% and 90% hydrogen utilization, respectively. The straight line is drawn by use of the results obtained from Fig. 6. The cell voltage showed little change in the case of 80% hydrogen utilization. But in the case of 90% hydrogen utilization the cell voltage changed noticeably with the average potential shift. Most of the points lie well on a straight line. This indicates that the influence of the average potential shift on the current distribution in the plane of a cell can be treated in a quantitative manner instead of the difference of gas flow configurations. The A1 type shows the highest potential shift and the lowest cell voltage indicating that CROSS-FLOW is the worst type of gas flow of the thirteen types, though it is the simplest configuration. RETURN-FLOW (C1, C2), CO-FLOW (D1) or COUNTER-FLOW (D2) can improve the potential shift and cell voltage significantly compared to CROSS-FLOW. However, the E2 type and the F2 type are superior to them.

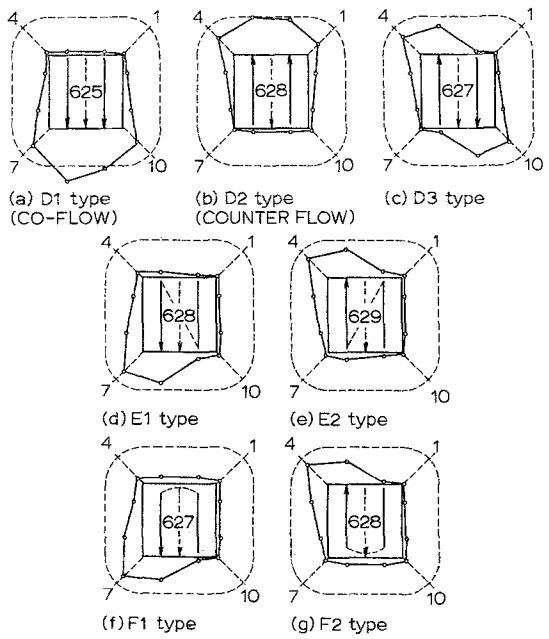

Fig. 9. Schematic diagrams showing anode potential distribution in a plane for the case of AIR ∥ FUEL.

4. Discussion

4.1. *Relation between potential shift and cell voltage*

In all cases shown in Fig. 8 and Fig. 9, the locations where significant potential shifts were observed lie in the fuel outlet area. In both cases of A2 and D3, the potential shifts were significant in the fuel outlets; this means that the potential shift was always located in the fuel outlet area irrespective of the types.

The change of RHE potentials measured by using a single cell with four reference electrodes has been reported [12, 13]. In these studies, it was observed that the potentials of the RHE in the fuel outlet area shift in the negative direction compared with RHE in the fuel inlet area when the potential shifts of the anode and the cathode occurred. The potential shift of RHE always had the same value as the potential shift of the anode and the cathode. In several cases, the voltages between an RHE and the other RHE was measured. As expected, the potential shifts of RHE near the fuel outlet were observed compared to the RHE near the fuel inlet. The potential shift of RHE always had the same value as the potential shift of the electrodes. Namely, the potential shifts of the electrodes were due to the change of the RHE potentials in the negative direction.

Figure 11 shows the potential of the anode, the cathode and RHE (equal to the redox potential of hydrogen: H^+/H_2 (0 V against RHE at 190° C)) in the fuel outlet area with respect to that of RHE at the fuel inlet area. The calculated oxygen evolution potentials (H^+, O_2/H_2O (1.14 V against RHE at 190° C)) are also given. The figure shows that the cathode or the anode potentials in the fuel inlet and the fuel

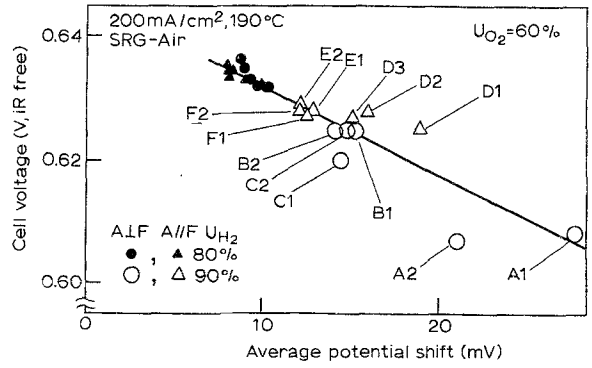

Fig. 10. The relation between average potential shift and cell voltage for the thirteen flow types.

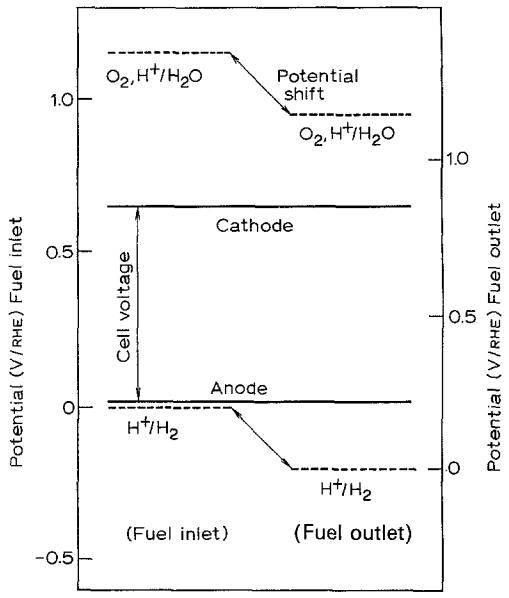

Fig. 11. A diagram giving the potential of cathode, anode and the redox potentials for H^+/H_2 and H^+, O_2/H_2O at fuel inlet and fuel outlet.

outlet are constant. On the other hand, the redox potentials of hydrogen (H^+/H_2) and oxygen evolution (H^+, O_2/H_2O) change between the inlet and outlet area. The cathode and anode potentials in the fuel outlet area can be understood as shifting in the positive direction against RHE compared with those of the fuel inlet area. On the other hand, the RHE potential in the fuel outlet area is understood as shifting in the negative direction compared with that of the fuel inlet area. Because the redox potential of H^+/H_2 or H^+, O_2/H_2O changes with pH of the electrolyte (the change is 59 mV/pH at 25° C and 92 mV pH at 190° C [17]), the shifts of the redox potentials in the fuel outlet area can be explained if the acidity of the electrolyte in the fuel outlet changes toward basic compared with that in the fuel inlet area.

Though data on the acidity of concentrated phosphoric acid at high temperature is limited, Dowing *et al.* [18] reported the acidity at 25° C to 27° C as $Ho = -4.1$ at 90% H_3PO_4, $Ho = -4.8$ at 100% H_3PO_4 and $Ho = -5.7$ at 110% H_3PO_4, where Ho is the Hammett acidity function. Namely concentrated phosphoric acid is a 'super acid', and at high temperature, phosphoric acid must remain a 'super acid'. The starvation of hydrogen in the fuel outlet area causes the acidity change in the electrolyte. If sufficient proton generation does not occur in the fuel outlet area, the acidity of the electrolyte should move toward less acidic values. For example, if the acidity of the electrolyte in the fuel outlet area changes locally from $Ho = -5$ to $Ho = 0$, the liquid junction potential between the fuel outlet area and the fuel inlet area becomes about 0.46 V (0.092×5). However, if the electrical resistance and the ionic resistance between the fuel inlet area and the fuel outlet area are small enough, the acidity change can be nullified by the migration of electrons and protons. However, the diffusion of protons is insufficient because the cell area is significantly large compared with the thickness of the matrix layer.

The influence of the potential shift (E_{sh}) on both the cathode and anode potentials (E_c, E_a) can be defined by the following equations

$$E_c(\text{V/RHE}) = E[H^+, O_2/H_2O] + (RT/2F) \times (\ln (P_{O_2}^{1/2}/P_{H_2O})) - \eta_c + E_{sh} \quad (1)$$

$$E_a(\text{V/RHE}) = E[H^+/H_2] - (RT/2F)(\ln (P_{H_2})) + \eta_a + E_{sh} \quad (2)$$

where η_c and η_a are the overpotentials of the cathode and the anode, respectively.

If the pH of electrolyte is constant in the plane of a cell, E_{sh} is zero. If the pH of the electrolyte changes locally in the fuel outlet area, E_{sh} becomes positive (92 mV/pH) and the cathode potential becomes high in the fuel outlet area. Then, η_c in the fuel outlet area should decrease compared with that in the fuel inlet area. This indicates the change of current distribution, that is, current convergence into the fuel inlet area. That is, as the current decreases in the fuel outlet area, so the current must increase in the fuel inlet area. The polarization of th cathode thus increases in the fuel inlet area. In Fig. 5 at 90% H_2 utilization, the cathode polarization of the cathode thus increases in the fuel (R3–R8); conversely in the fuel inlet area (R9–R12, R1–R2), the cathode polarization seems to increase. The decrease of cell voltage by the increase of hydrogen utilization was caused, not only by the increase of anode polarization, but also by the increase in cathode polarization, because both polarizations were increased by current convergence into the fuel inlet area.

The linear relation between the average potential shift and cell voltage in Fig. 6 indicates that current convergence into the fuel inlet area increases with increase of potential shift. The linear relation between the average potential shift and cell voltage is also obtained in Fig. 10. The different results for the thirteen types of fuel gas flow can be attributed to the current distribution in the horizontal plane of a cell.

It is difficult to determine the current distributions in a quantitative manner from this work. In order to understand the current distributions, further investigation, including some computer modelling studies, is necessary.

4.2. *A comparison of the thirteen flow types*

In Fig. 10, there is little change throughout the thirteen flow types for 80% hydrogen utilization. However, for 90% hydrogen utilization, noticeable differences appear among them; this is due to the difference of the potential shift and the current distribution in the horizontal plane of a cell. If the potential shift is small, the current distribution will be nearly homogeneous. Conversely, if the potential shift is large, the current convergence into the fuel inlet area will become remarkable.

The supply of excess hydrogen is the most effective method for decreasing the potential shift. For example, the direction of fuel and air flows of type B1 or type B2 is exactly equal to that of type A1, but the potential shift of the former was lower than that of the latter type. The difference between type B1 (B2) and type A1 lies in the fact that the fuel is used twice in the former, but only once in the latter. In the upstream space (for example, the upper space where Fuel 1 flows in Fig. 2) of type B1, the actual hydrogen utilization in the fuel is lower than that of type A1, because excess hydrogen is supplied to the downstream space (the lower space in Fig. 2). Then, in the downstream space, the actual hydrogen utilization is also lower than that of type A1, because the unused hydrogen in the upstream space is supplied to the downstream space. Namely, the starvation of hydrogen hardly occurs in type B1 or B2 (Condition 1). A similar tendency is expected for type A2 and type C2, for type D1 and type E1, for type D2 and type E2, and for type D3 and type F2.

When the 'AF cross cells' are compared with the 'AF parallel cells' at 80% hydrogen utilization, there is little difference in the cell performance or potential shift in all the thirteen flow types. However, in the cases at 90% hydrogen utilization, the 'AF parallel cells' were superior to the 'AF cross cells'. In the cases of 'AF parallel cells', fuel is supplied from the air inlet area to the air outlet area, or from the air outlet area to the air inlet area. However, in the cases of 'AF cross cells', fuel is supplied only to the air inlet area or to the air outlet area. If the imbalance of current density in the horizontal plane of a cell is significant between the air inlet area and the air outlet area, the starvation of hydrogen easily occurs in the cases of 'AF cross cells'. However, in the cases of 'AF parallel cells', the starvation of hydrogen due to the same reason hardly occurs because the fuel gas flow is parallel with the air flow (Condition 2). Accordingly the 'AF parallel cells' are better than the 'AF cross cells'.

Among the 'AF cross cells', RETURN-FLOW (C1, C2) is better than CROSS-FLOW (A1). However, many of the 'AF parallel cells' are superior to the RETURN-FLOW (C1, C2).

Among the 'AF parallel cells', COUNTER-FLOW (D2) is better than CO-FLOW (D1). In the case of CO-FLOW, current is concentrated to the inlet area of fuel and air. However, in the case of COUNTER-FLOW, current is dispersed homogeneously in the horizontal plane, because the fuel gas flow is opposite to the air flow (Condition 3).

Type E2 and type F2 are superior to the COUNTER-FLOW (D2), and type E2 is the best. The E2 type surpasses others for several reasons. Firstly, it enables the use of fuel twice (Condition 1), this is superior to type D2. Secondly, it is the 'AF parallel cell' (Condition 2), which is superior to the 'AF cross cell'. Thirdly, type E2 is similar to COUNTER-FLOW (Condition 3), which is superior to type E1 (E1 is similar to CO-FLOW type). Types F1 and F2 are the intermediate types between COUNTER-FLOW and CO-FLOW which are inferior to type E2.

The degree of satisfaction for the three conditions for each of the thirteen flow types is summarized in the last column of Table 1, where the symbols ○, × and △ mean that the condition is satisfied, not satisfied or partly satisfied, respectively.

In conclusion, experimental results show that the cell performance increased and the potential shift decreased under high fuel utilization conditions in the following order; CROSS-FLOW < RETURN-FLOW = CO-FLOW < COUNTER-FLOW < type E2. Unfortunately, it seems that the type E2 is too complicated to fabricate. The extent of the change among the various types depended on the above three conditions.

Acknowledgement

This work was conducted under the Moonlight project and was carried out under contract with the New Energy and Industrial Technology Development Organization (NEDO), Japan.

References

[1] P. E. Grevstad, C. K. Johnson and A. P. Mientek, US Patent 4 337 571 (1982).
[2] O. J. Adlhart, US Patent 4 175 165 (1979).
[3] H. R. Kunz and C. A. Reiser, US Patent 3 994 748 (1976).
[4] Y. Seta, M. Ueno, K. Murata and T Shirogami, The Electrochemical Society of Japan 49th Meeting abstracts (1982) No. B219.
[5] W. H. Johnson, US DoE Technical Progress Report No. 2, 'Improvement of Fuel Cell Technology Base', Contract No. ET-76-C-03-1169 (1978).
[6] T. Watanabe, Y. Mugikura, Y. Izaki, N. Horiuchi, T. Matsuyama, E. Kasai and S. Sato, Fuel Cell Seminar, abstracts (1988) p. 300.
[7] A. Suzaki, M. Hosaka, H. Kasai, Y. Yamasu, M. Hotta, K. Watanabe and S. Sato, Fuel Cell Seminar, abstracts (1988) p. 386.
[8] H. Ide, M. Matsumura, T. Taniguchi, K. Mitsuda and E. Nishiyama, Spring Meeting of The Institute of Electrical Engineers of Japan, abstracts (1984) No. 1065.
[9] V. Sampath, A. F. Sammells and J. R. Selman, *J. Electrochem. Soc.* **127** (1980) 79.
[10] T. L. Wolf and G. Wilemski, *ibid.* **130** (1983) 48.
[11] K. Mitsuda, H. Ide and T. Murahashi, Spring Meeting of The Institute of Electrical Engineers of Japan, abstracts (1989) No. 1544.
[12] K. Mitsuda, H. Shiota, J. Aragane and T. Murahashi, The Electrochemical Society 174th Meeting, Chicago, abstracts (1988) No. 52.
[13] K. Mitsuda and T. Murahashi, *J. Electrochem. Soc.* **137** (1990) 3079.
[14] K. Mitsuda and T. Murahashi, The 40th Meeting of International Society of Electrochemistry, Kyoto, abstracts (1989) No. b1-18-01-13-G.
[15] K. Mitsuda and T. Murahashi, submitted to this journal.
[16] K. Mitsuda, H. Shiota and T. Murahashi, *Corrosion* **46** (1990) 628.
[17] M. Pourbaix, 'Atras D'Eqibres Electrochimiques', Gauthie-Villars (1963) p. 102.
[18] R. G. Dowing and D. E. Peason, *J. Am. Chem. Soc.* **83** (1961) 1718.